CMS Physics Analysis Summary

Contact: cms-pag-conveners-b2g@cern.ch 2017/07/11

Search for pair production of excited top quarks in the lepton+jets final state

The CMS Collaboration

Abstract

A search is performed for pair production of spin-3/2 excited top quarks, each decaying to a top quark and a gluon. The search uses the data collected with the CMS detector from pp collisions at a center-of-mass energy of $\sqrt{s} = 13\,\text{TeV}$, corresponding to an integrated luminosity of $36\,\text{fb}^{-1}$. The selected events require the presence of an isolated muon or electron, an imbalance in the transverse momentum, and at least six jets, out of which exactly two must be compatible with originating from the fragmentation of a b quark. The analysis shows no significant excess over the standard model predictions, and provides a lower limit of 1.2 TeV at 95% confidence level on the mass of the spin-3/2 excited top quark in an extension of the Randall–Sundrum model, assuming a 100% branching fraction of its decay into a top quark and a gluon.

1 Introduction

The standard model (SM) of particle physics provides a very successful description of the properties of the particles of nature and their interactions. Despite its success, the SM is known to not be a fundamental theory, but is assumed to be an effective model of a more complete theory. Many extensions of the SM predict that the top quark is a composite particle and not a fundamental object [1–4]. A direct confirmation of this hypothesis could be achieved by the discovery of an excited top quark (t^*).

In models that describe the proposed excited top quark [5, 6], weak isodoublets are used to represent both left-handed and right-handed components of the t^* quark, allowing for finite masses prior to the onset of electroweak symmetry breaking. Thus, in contrast to the heavy top quark from a sequential fourth generation model, the existence of t^* quarks is not strongly limited by the discovery of a SM-like Higgs boson [7–9]. In string realizations of the Randall–Sundrum (RS) model [10, 11], the right-handed t^* quark is expected to be the lightest spin-3/2 excited state [12].

A spin-3/2 excited top quark is described by the Rarita–Schwinger [13] vector-spinor Lagrangian. The production cross section of spin-3/2 quarks is proportional to $\hat{s}^3$, where $\hat{s}$ is the square of the energy in the parton-parton collision rest frame. This differs from the production cross section of spin-1/2 quarks which is proportional to $\hat{s}^{-1}$. Therefore, when integrating over the parton momentum fractions (x) in proton-proton collisions, spin-3/2 quarks receive an increased contribution from large x values compared to spin-1/2 quarks. The spin-3/2 t^* quark in the RS model is expected to have a pair production cross section of the order of a few pb at $\sqrt{s} = 13\,\text{TeV}$ for a t^* of mass $m_{t^*} = 1\,\text{TeV}$ [1, 14, 15]. This cross section is calculated at leading order in perturbation theory, with the factorization and renormalization scales set to $Q = m_{t^*}$. The t^* quark decays predominantly to a top quark through the emission of a gluon [1, 12, 14, 16].

In this paper, we present a search for pair produced t^* quarks, where each t^* quark decays exclusively to a top quark (t) and a gluon (g). We use data recorded in 2016 with the CMS detector in proton-proton (pp) collisions at $\sqrt{s} = 13\,\text{TeV}$ at the LHC, corresponding to an integrated luminosity of $36\,\text{fb}^{-1}$. We consider the case where one top quark decays via a hadronically decaying W boson, and the W boson from the second top quark decays to a electron or muon and a neutrino: $t^*\bar{t}^* \to (tg)(\bar{t}g) \to (W^+bg)(W^-\bar{b}g) \to (q_1q_2bg)(l\bar{\nu}\bar{b}g)$. We refer to the resulting final state (one reconstructed muon or electron, missing transverse momentum, and multiple jets) as the lepton+jets decay topology.

A search for pair produced excited top quarks was previously performed by CMS using pp collisions at $\sqrt{s} = 8\,\text{TeV}$ [17]. This result presents a more sensitive search due to the larger collision energy and therefore larger signal cross sections. Also, the signal simulation has been improved as the Rarita-Schwinger Lagrangian has been included in the signal generator.

2 The CMS Detector and Simulated Samples

The central feature of the CMS apparatus is a superconducting solenoid of 6 m internal diameter, providing a magnetic field of 3.8 T. Within the solenoid volume are a silicon pixel and strip tracker, a lead tungstate crystal electromagnetic calorimeter (ECAL), and a brass and scintillator hadron calorimeter (HCAL), each composed of a barrel and two endcap sections. Forward calorimeters extend the pseudorapidity coverage provided by the barrel and endcap detectors. Muons are measured in gas-ionization detectors embedded in the steel flux-return yoke out-

side the solenoid. A more detailed description of the CMS detector, together with a definition of the coordinate system used and the relevant kinematic variables, can be found in Ref. [18].

Simulated signal $t^*\bar{t}^*$ events are generated with m_{t^*} 700–1600 GeV in 100 GeV steps using the MADGRAPH 5 [19] event generator and the NNPDF3.0 [20] for the parton distribution functions. The cross section ranges from $\approx$ 5 pb down to $\approx$ 4 fb depending on the signal mass. The Rarita–Schwinger Lagrangian, included in the MADGRAPH 5 generator, is used for simulating spin-3/2 $t^*\bar{t}^*$ events. Parton shower and hadronization processes are modeled using PYTHIA 8 [21]. The generated events are processed through a simulation of the CMS detector based on GEANT4 [22], and reconstructed using the same algorithms as used for data.

We estimate SM backgrounds using a data-derived approach. Simulated samples for SM processes are used to study the modeling of the background and to provide a cross-check of the analysis procedures. The simulated SM samples relevant to this analysis are $t\bar{t}$ production, single top quark production via the s channel, t channel, and tW processes, W and Z boson production in association with jets, and the $t\bar{t}+W$, $t\bar{t}+H$, and $t\bar{t}+Z$ processes. The $t\bar{t}$ and $t\bar{t}+H$ processes are simulated using POWHEG [23–27], while the other SM processes are simulated using MADGRAPH up to next-to-leading order [28–30]. All simulated samples include the additional contributions from overlapping pp collisions within the same and nearby bunch crossing ("pileup") at large instantaneous luminosity. The simulation is weighted to match the distribution of the average number of pileup interactions in data.

3 Event reconstruction

Event reconstruction is based on the CMS particle-flow (PF) algorithm [31], which takes into account information from all subdetectors, including measurements from the tracking system, energy deposits in the ECAL and HCAL, and tracks reconstructed in the muon detectors. Given this information, all particles in the event are reconstructed as electrons, muons, photons, charged hadrons, or neutral hadrons. Photons (e.g. coming from π^0 decays or from electron bremsstrahlung) are identified as ECAL energy clusters not linked to the extrapolation of any charged particle trajectory to the ECAL. Electrons (e.g. coming from photon conversions in the tracker material or from b-hadron semileptonic decays) are identified as a primary charged particle track and potentially many ECAL energy clusters corresponding to this track extrapolation to the ECAL and to possible bremsstrahlung photons emitted along the way through the tracker material. Muons (e.g. from b hadron semileptonic decays) are identified as a track in the central tracker consistent with either a track or several hits in the muon system, associated with an energy deficit in the calorimeters. Charged hadrons are identified as charged particle tracks neither identified as electrons, nor as muons. Finally, neutral hadrons are identified as HCAL energy clusters not linked to any charged hadron trajectory, or as ECAL and HCAL energy excesses with respect to the expected charged hadron energy deposit.

For each event, hadronic jets are clustered from these reconstructed particles with the infrared and collinear safe anti-k_T algorithm [32] with a size parameter R of 0.4. Charged hadrons associated to a pileup vertex are excluded from those used in jet reconstruction. Jet momentum is the vectorial sum of the momenta of all particles contained in the jet. The reconstructed jet momentum is found in simulation to be within 5 to 10% of the true momentum over the whole p_T spectrum and detector acceptance. Jet energy corrections are derived from the simulation and data in situ measurements [33]. The jet energy resolution amounts typically to 15% at 10 GeV, 8% at 100 GeV, and 4% at 1 TeV. A smearing of the jet energy is applied to simulated events to mimic detector resolution effects observed in data.

Jets are identified as originating from a b quark through a combined secondary vertex (CSV) algorithm [34]. The algorithm uses a multivariate discriminator to combine information on the significance of the impact parameter, the jet kinematics, and the location of the secondary vertex. The working point of the discriminator with $\approx$ 70% b quark identification efficiency and $\approx$ 1% mistag efficiency is used in this analysis. Small differences in b tagging efficiencies and mistag rates between data and simulated events are accounted for by applying additional corrections to simulation.

The missing transverse momentum vector is defined as the negative vector sum of the momenta of all reconstructed particles in an event projected on the plane perpendicular to the beams. Its magnitude is referred to as $E_{\mathrm{T}}^{\mathrm{miss}}$.

4 Event Selection

This analysis searches for $\mathrm{t}^*\bar{\mathrm{t}}^*$ production, with each t^* decaying to $\mathrm{t}+\mathrm{g}$ and the $\mathrm{t}\bar{\mathrm{t}}$ pair in the event reconstructed in the lepton+jets final state. Events are required to contain exactly one isolated lepton, missing transverse momentum and at least 6 jets, exactly two of which must be b-tagged.

Events containing a muon are selected with a single-muon trigger, requiring the presence of an isolated muon with transverse momentum $p_{\mathrm{T}} > 27\,\mathrm{GeV}$. Events containing an electron are selected with a single-electron trigger, requiring the presence of an isolated electron with $p_{\mathrm{T}} > 32\,\mathrm{GeV}$.

Muons are required to have $p_{\mathrm{T}} > 30\,\mathrm{GeV}$, and pseudorapidity $|\eta| < 2.1$. The track associated with a muon is required to have hits in the pixel and muon detectors, a good quality fit, and transverse and longitudinal impact parameters with respect to the primary vertex smaller than 2 mm and 5 mm respectively. An isolation factor I is defined as the sum of the p_{T} of all photons, charged hadrons and neutral hadrons within an angular cone of $\Delta R \equiv \sqrt{(\Delta\eta)^2 + (\Delta\phi)^2} < 0.4$ around the track corrected for the effects of pileup [35], divided by the muon p_{T}. A tight isolation selection $I < 0.15$ corresponding to an efficiency of $\approx$ 95% is used.

The electrons are required to have transverse momentum $p_{\mathrm{T}} > 35\,\mathrm{GeV}$, and be within the region $|\eta| < 2.1$. Rejection of electrons within the region $|\eta| \in [1.44, 1.56]$, corresponding to the ECAL barrel–endcap transition region, is employed to avoid poor reconstruction performances. Electrons are selected using the cut-based selection method described in Ref. [36] based on the shower-shape, the track quality, the spatial match between the track and the electromagnetic cluster, the fraction of total cluster energy in the HCAL, and the resulting level of activity in the surrounding tracker and calorimeter regions. A tight working point corresponding to an efficiency of $\approx$ 70% is used.

In addition to the selections above, the leptons are required have an angular separation $\Delta R < 0.1$ with respect to the lepton reconstructed by the trigger system. The lepton selection efficiencies for data and simulation are measured using the tag-and-probe method [36]. Additional corrections are applied to simulation to account for remaining differences in the efficiencies between data and simulation.

The missing transverse momentum $E_{\mathrm{T}}^{\mathrm{miss}}$ is required to be greater than 20 GeV, while the jets are required to have $p_{\mathrm{T}} > 30\,\mathrm{GeV}$, $|\eta| < 2.4$, and angular separation $\Delta R > 0.4$ with respect to well-identified electrons or muons. In order to reject fake, badly reconstructed and noise jets, the energy contribution of the constituent charged hadron particles, neutral hadron particles, changed EM particles and neutral EM particles to the total jet energy must be non-zero and

Table 1: Summary of the expected number of events after event selection for the simulated signal process and SM processes, as well as the number of selected events observed in data. Uncertainties in the expected number of events predicted by the standard model include the systematic uncertainties discussed in Section 7, as well as uncertainties in the cross sections of the various processes.

	μ+jet final state	e+jet final state
$t^*\bar{t}^*(M_{t^*} = 700\,\text{GeV})$	3666	2726
$t^*\bar{t}^*(M_{t^*} = 800\,\text{GeV})$	1230	1014
$t^*\bar{t}^*(M_{t^*} = 900\,\text{GeV})$	483	369
$t^*\bar{t}^*(M_{t^*} = 1000\,\text{GeV})$	200	148
$t^*\bar{t}^*(M_{t^*} = 1100\,\text{GeV})$	92	69
$t^*\bar{t}^*(M_{t^*} = 1200\,\text{GeV})$	40	29
$t^*\bar{t}^*(M_{t^*} = 1300\,\text{GeV})$	20	15
$t^*\bar{t}^*(M_{t^*} = 1400\,\text{GeV})$	9	7
$t^*\bar{t}^*(M_{t^*} = 1500\,\text{GeV})$	4	4
$t^*\bar{t}^*(M_{t^*} = 1600\,\text{GeV})$	2	2
SM processes	$(4.66 \pm 0.38) \times 10^4$	$(3.07 \pm 0.23) \times 10^4$
Data	44 573	28 942

non-unity. Exactly two jets are required to pass the b tagging criteria.

Simulated signal events pass the selection criteria with an efficiency of 1.4–2.2%, depending on the channel and on the signal m_{t^*}. After the application of all selections, 44 573 events are observed in the μ + jets channel and 28 942 events in the e + jets channel. The yields predicted from the simulated standard model background processes are 46 895 events in the μ + jets channel and 30 743 events in the e + jets channel. Small differences in data relative to the standard model predictions are within the estimated uncertainties of simulation, with the dominant uncertainty being the choice of the renormalization and factorization scales used in the generator of the $t\bar{t}$ events. Details of the uncertainties will be given in Section 7. Furthermore, the differential distributions of kinematic variables of simulated SM processes are also in good agreement with data, as shown in Figure 1. In particular, the distribution of the invariant mass of a t + jet system (see Section 5 for details) in data is in good agreement with the background estimation.

5 Mass reconstruction

Since the dominant background is SM $t\bar{t}$ production with extra jets, the reconstructed invariant mass spectrum of the t + jet systems is used to distinguish between $t^*\bar{t}^*$ signal and $t\bar{t}$ background. Given the high jet multiplicity of the event selection, a measure must be designed to determine how reconstructed jets should be associated to the parton level object in the final state.

The E_T^{miss} is assumed to be carried away entirely by the neutrino from the leptonically decaying W boson. We assume that the parent W boson is on shell and the neutrino is effectively massless in order to solve for the longitudinal momentum of the neutrino.

For the jets, just the six leading jets are taken into consideration. The goodness of the jet–parton assignment for a single event with b-tagged jets assigned to one of the b quark partons, is evaluated with an S value computed based on how well the intermediate physical objects

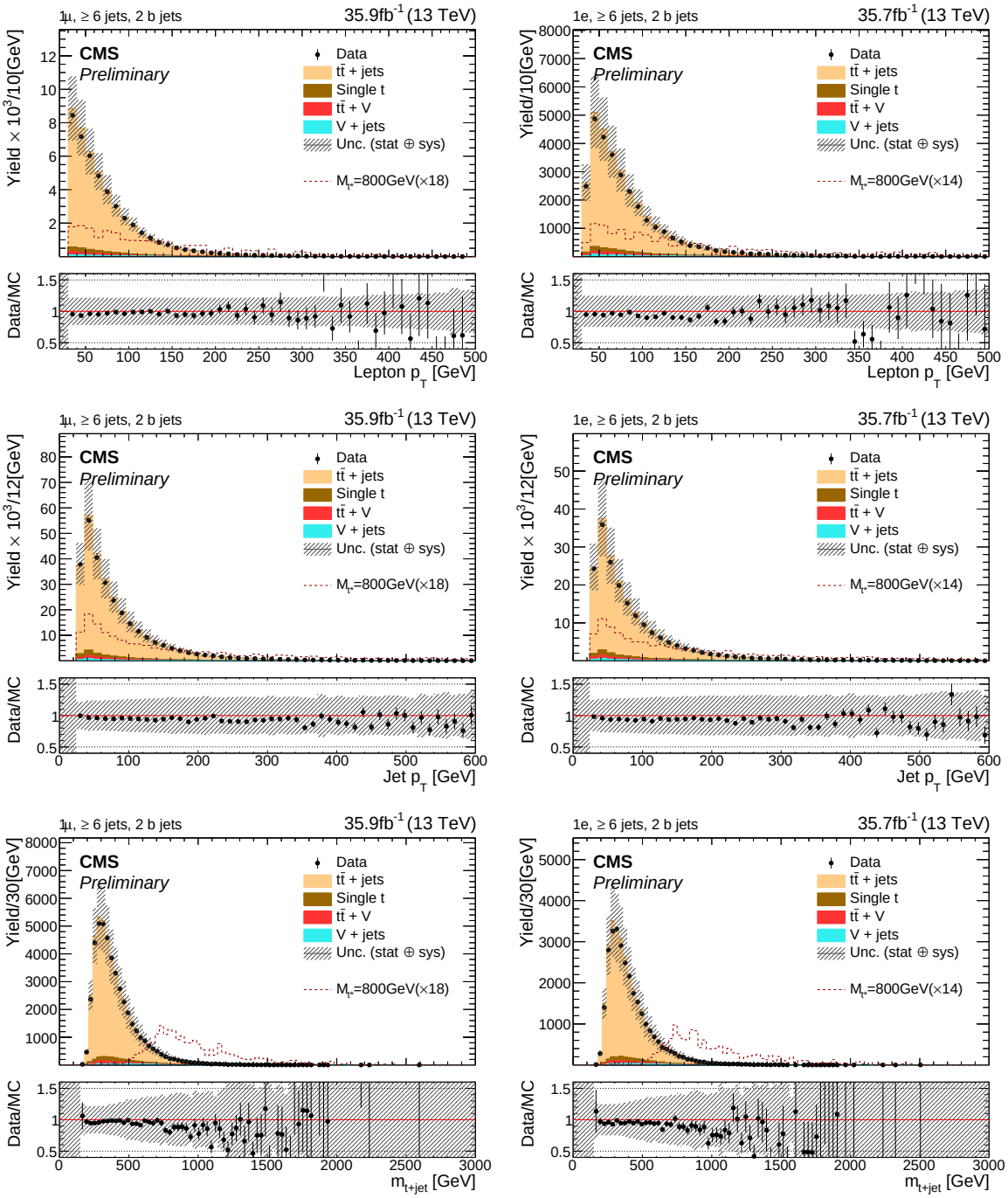

Figure 1: Kinematic distributions of events selected with a single lepton, ≥ 6 jets with exactly two b tagged jets in data (points), simulated background processes (stacked histograms), and simulated 800 GeV signal process (dashed line). Events selected in the μ(e)+jet final state are shown on the left (right). From top to bottom, the kinematic variable displayed are the lepton p_{T} spectra, the jet p_{T} spectra and the $m_{\mathrm{t+jet}}$ spectra. The shaded region is the total uncertainty of the simulated background processes, which includes statistical and systematic uncertainties.

are reconstructed:

$$S = \left(\frac{m_{\mathrm{q\bar{q}'}} - M_{\mathrm{W}}}{\sigma_{\mathrm{W}}}\right)^2 + \left(\frac{m_{\mathrm{q\bar{q}'b}} - M_{\mathrm{t}}}{\sigma_{\mathrm{t,had}}}\right)^2 + \left(\frac{m_{\ell\nu_\ell \mathrm{b}} - M_{\mathrm{t}}}{\sigma_{\mathrm{t,lep}}}\right)^2 + \left(\frac{m_{\mathrm{q\bar{q}'bg}} - m_{\ell\nu_\ell \mathrm{bg}}}{\sigma_{\mathrm{t^*}}}\right)^2 . \quad (1)$$

M_{W} and M_{t} are the mass of the W boson and t quark recorded by the particle data group (PDG) [37], being 80.4 GeV and 173.34 GeV, respectively. The expected detector resolution of the intermediate particles σ_{W}, $\sigma_{\mathrm{t,had}}$, $\sigma_{\mathrm{t,lep}}$ and $\sigma_{\mathrm{t^*}}$ are estimated to be 24.1, 33.7, 30.2 and 233.5 GeV, respectively. These estimates are obtained by reconstructing the $\mathrm{t^*\bar{t}^*}$, $\mathrm{t\bar{t}}$ and $\mathrm{W_{had}}$ in the decay topology using the truth information from simulated signal samples. Additional studies have shown that the reconstruction is not sensitive to changes in the value of detector resolution.

The jet–parton assignment with the smallest S value is taken to represent the decay topology of a single event under the t* hypothesis. The average value of the $m_{\mathrm{q\bar{q}'bg}}$ and $m_{\ell\nu_\ell \mathrm{bg}}$ computed for said assignment is taken to represent the reconstructed t* mass of an event, notated as $m_{\mathrm{t+jet}}$.

6 Background modeling and extraction of t* signal

To determine the presence of signal events in data, an unbinned extended maximum-likelihood fit of a signal-plus-background model is performed on the $m_{\mathrm{t+jet}} > 400$ GeV spectrum.

The spectrum template of the $\mathrm{t^*\bar{t}^*}$ signal is constructed from simulation using an adaptive kernel estimation [38] with a Gaussian kernel and no restriction on the spectrum boundary. The smoothness parameter ρ introduced in Ref. [38] is determined by the square root of the standard deviation of the signal spectrum over the subset with ≥ 4 correctly assigned partons.

The spectrum of the background is modeled using a log-normal function (up to a normalization factor):

$$f_{\mathrm{bkg}}(m) = \frac{1}{m\sqrt{2\pi}} \exp\left(-a_2 \ln^2\left(\frac{m}{m_0}\right)\right) \quad (2)$$

where m is the mass, and a_2 and m_0 are the parameters that determine the shape of the background. During the fit to the observed data, the number of background events, as well as the shape parameters of the background function, are left floating.

To verify whether the fit is sensitive to the presence of $\mathrm{t^*\bar{t}^*}$ signal, a pseudo data-set is generated with the $m_{\mathrm{t+jet}}$ spectrum of the simulated backgrounds and then injected with the expected $m_{\mathrm{t+jet}}$ signal spectrum for various hypotheses of the signal cross section. Performing the same fit over multiple sets of pseudo data with varying signal cross sections, particularly with the signal cross section set to the theoretical prediction of the R–S model or 0, showed no evidence of bias.

To ensure that the log-normal function is sufficient to model the background, a likelihood ratio test is conducted by comparing the results of fitting the spectrum of simulated SM background to extended log-normal function in the form of:

$$f_{\mathrm{bkg},N}(m) = \frac{1}{m\sqrt{2\pi}} \exp\left(-a_2 \ln^2\left(\frac{m}{m_0}\right) - a_3 \ln^3\left(\frac{m}{m_0}\right) - \ldots - a_N \ln^N\left(\frac{m}{m_0}\right)\right) \quad (3)$$

It is found that increasing the number of parameters does not improve the description of the background.

The results of the fit performed on data with the 800 GeV signal spectrum are shown in Figure 2. The number of events in data is in good agreement with a null hypothesis. No significant evidence of $\mathrm{t^*\bar{t}^*}$ production is found.

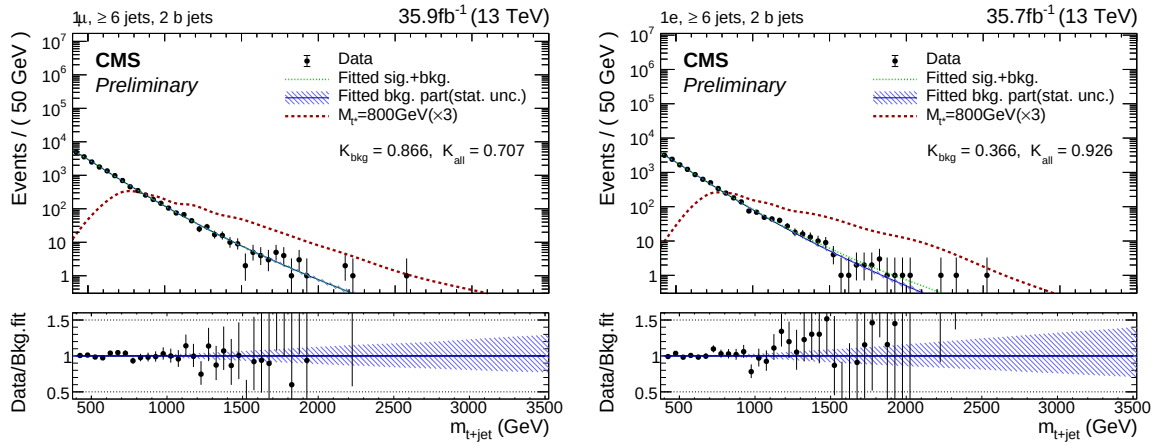

Figure 2: The $m_{\mathrm{t+jet}}$ spectrum for data (points), the signal+background fit (green), the background component of the signal+background fit (blue), and the expected spectrum for 800 GeV signal process (red dashed) normalized to the integrated luminosity of data. The plot on the left (right) shows the distributions for the μ+jets (e+jets) data. The probability of the Kolmogorov–Smirnov test between the data versus the signal+background model, and data versus the background component is notated K_{all} and K_{bkg} respectively.

7 Systematic uncertainties

The impact of experimental and theoretical sources of uncertainties are considered. For each source of uncertainty, alternative templates for the distribution of $m_{\mathrm{t+jet}}$ are generated by adjusting the relevant parameters in the simulation.

The uncertainties in the jet energy scale and jet resolutions are dependent on the p_{T} and η of the jets. The alternative spectrum templates are generated by rescaling the nominal jet four-momentum in the simulation by ± 1 standard deviation of the associated uncertainties in energy scale and resolution. Such uncertainties are also coherently propagated to all observables including $E_{\mathrm{T}}^{\mathrm{miss}}$. Varying the jet energy used for reconstruction has $< 0.1\%$ impact on the signal acceptance.

The b tagging and lepton selection scale factors for residual differences between data and simulation have their respective systematic and statistical uncertainties. Alternative templates are generated by shifting the correction scale factors by ± 1 standard deviation for their respective uncertainties. On average, the b tagging scale factor and lepton scale factors affect the signal acceptance by 2.8% and 7.0%, respectively. Because of uncertainties in the total inelastic pp cross section when calculating the data pileup scenario, alternative pileup corrections are made with the inelastic cross section scaled by ± 1 standard deviation. Variations in the pileup corrections has an average impact on the signal acceptance of 0.7%. The number of signal events is also affected by the uncertainty on the integrated luminosity, which is known to a precision of 2.5%.

The theoretical uncertainties considered are the choice of the PDF and the renormalization and factorization scales used by the event generator. Effects of the theoretical uncertainties are obtained by changing the various generator parameters within their estimated uncertainties and generating new $m_{\mathrm{t+jet}}$ fit templates that are used to calculate new sensitivities.

In addition to the statistical uncertainty originating from the signal+background fit, systematic uncertainties are introduced to cover the choice of modeling. Alternative signal templates are generated with different smoothing parameters ρ by changing the subset to require ≥ 3 and ≥ 5 correctly assigned partons. Since the background is determined by entirely data derived

methods, no additional systematic is associated with the background modeling.

Table 2: List of systematic uncertainties affecting the signal m_{t+jet} templates. (S.D. — standard deviation, S.F. — correction scale factor)

Source of uncertainty	Effect on simulated signal sample
Integrated luminosity	Normalization shift by $\pm 2.5\%$
Statistical uncertainty	Normalization shift by ± 1S.D.
Jet correction	Correction factor varied by ± 1S.D.
Jet resolution	Jet energy shift by ± 1S.D.
b tagging S.F.	S.F. varied by ± 1S.D.
Lepton efficiency S.F.	S.F. varied by ± 1S.D.
Pileup	pp cross section shifted by $\pm 4.6\%$
Modeling	Vary smoothing parameter ρ in $[1.17, 1.66]$
PDF uncertainty	Generator parameter varied by ± 1S.D.
Scale uncertainty	Generator parameter varied by ± 1S.D.

8 Statistical analysis and extraction of limits

No excess above SM background is observed. We set an upper bound on the $t^*\bar{t}^*$ production cross section using the asymptotic modified frequentist CL_s method [39]. The null hypothesis likelihood function is taken from the background component of the signal+background fit described in Section 6. For the uncertainties described in Section 7, a joint template is used, where the nominal template is linearly interpolated to the templates generated with the relevant parameters shifted by ± 1 standard deviation. Each of the interpolation variables is taken as a nuisance parameter with a standard Gaussian prior.

The fit is performed separately in the muon and electron channel, and the results of the two are used to obtain combined limits. Figure 3 shows the observed and expected upper limits at 95% confidence level for the $t^*\bar{t}^*$ production. The lower limit for m_{t^*} is given by the value at which the upper limit intersects with the theoretical cross section from Ref. [15]. Both the observed and expected lower limit of m_{t^*} for the combined muon and electron data is 1.2 TeV within uncertainty.

9 Summary

A search for spin-3/2 $t^*\bar{t}^*$ production in pp interactions, with each t^* decaying exclusively to a standard model t quark and a gluon, has been conducted. Events that have a single muon or electron and at least six jets, exactly two of which must be identified as originating from a b quark, are selected for the analysis. Assuming $t^*\bar{t}^*$ production, an attempt is made to reconstruct the final state objects to a t^* candidate in each event. The observed mass spectrum of the $t + jet$ system shows no significant deviation from standard model predictions, and is used to set an upper limit on the production of $t^*\bar{t}^*$ as a function of t^* mass. By comparing the results with the expectations for a spin-3/2 excited top quark model, t^* masses below 1.2 TeV at 95% confidence level are excluded.

References

[1] H. Georgi, L. Kaplan, D. Morin, and A. Schenk, "Effects of top quark compositeness", *Phys. Rev. D* **51** (1995) 3888, doi:10.1103/PhysRevD.51.3888.

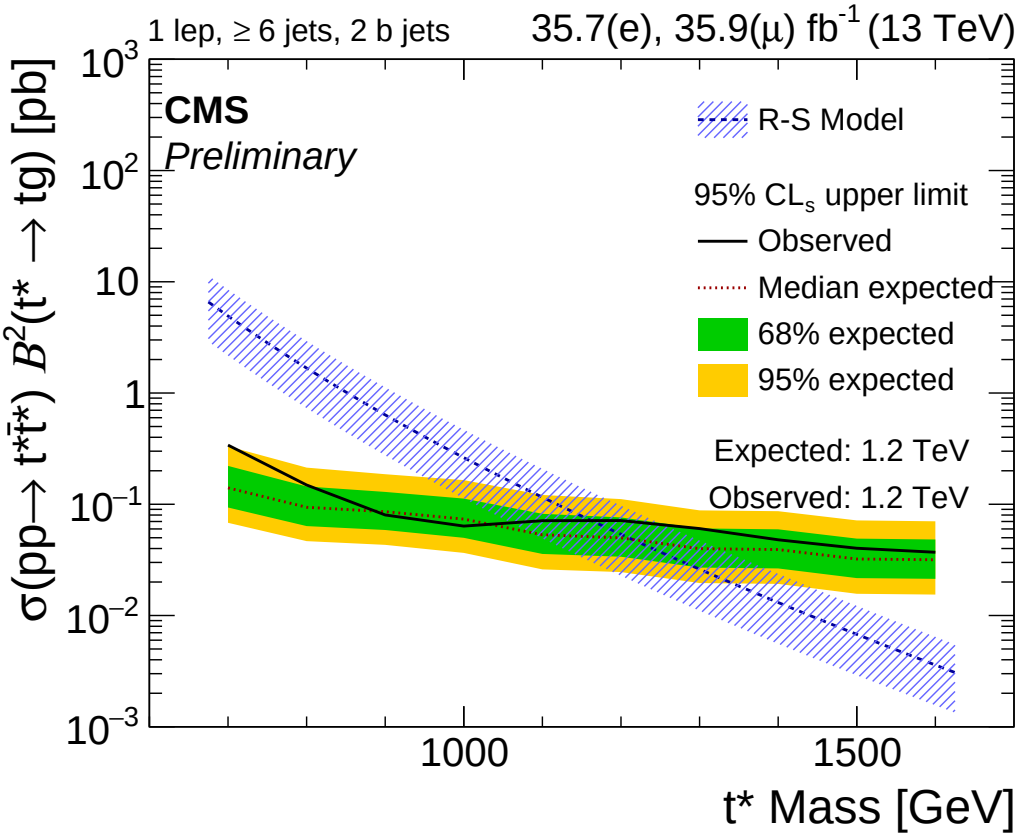

Figure 3: The expected (red dotted, and green-yellow double band region) and observed (black, solid) upper limit for the production cross section of $t^*\bar{t}^*$ versus t^*mass at 95% confidence level is presented for the combined lepton+jets analysis. The theoretical production cross section (blue hashed) is shown along with the uncertainties (blue hashed) on the signal acceptance as described in Section 7.

[2] B. Lillie, J. Shu, and T. M. P. Tait, "Top Compositeness at the Tevatron and LHC", *JHEP* **04** (2008) 87, doi:10.1088/1126-6708/2008/04/087, arXiv:0712.3057.

[3] A. Pomarol and J. Serra, "Top quark compositeness: Feasibility and implications", *Phys. Rev. D* **78** (2008) 74, doi:10.1103/PhysRevD.78.074026.

[4] K. Kumar, T. M. P. Tait, and R. Vega-Morales, "Manifestations of Top Compositeness at Colliders", *JHEP* **05** (2009) 22, doi:10.1088/1126-6708/2009/05/022, arXiv:0901.3808.

[5] U. Baur, M. Spira, and P. M. Zerwas, "Excited-quark and -lepton production at hadron colliders", *Phys. Rev. D* **42** (1990) 815, doi:10.1103/PhysRevD.42.815.

[6] R. M. Harris, "Discovery mass reach for excited quarks at hadron colliders", *eConf* **C960625** (1996) arXiv:hep-ph/9609319.

[7] ATLAS and CMS Collaborations , "Combined Measurement of the Higgs Boson Mass in pp Collisions at $\sqrt{s} = 7$ and 8 TeV with the ATLAS and CMS Experiments", *Phys. Lett.* **14** (2015) 191803, doi:10.1103/PhysRevLett.114.191803, arXiv:1503.07589.

[8] CMS Collaboration, "Observation of a new boson at a mass of 125 GeV with the CMS experiment at the LHC", *Phys. Lett. B* **716** (2012) 30, doi:10.1016/j.physletb.2012.08.021, arXiv:1207.7235.

[9] ATLAS Collaboration, "Observation of a new particle in the search for the Standard Model Higgs boson with the ATLAS detector at the LHC", *Phys. Lett. B* **716** (2012) 1, doi:10.1016/j.physletb.2012.08.020, arXiv:1207.7214.

[10] L. Randall and R. Sundrum, "An Alternative to Compactification", *Phys. Lett.* **3** (1999) 4690, doi:10.1103/PhysRevLett.83.4690.

[11] L. Randall and R. Sundrum, "Large Mass Hierarchy from a Small Extra Dimension", *Phys. Lett.* **3** (1999) 3370, doi:10.1103/PhysRevLett.83.3370.

[12] B. Hassanain, J. March-Russell, and J. G. Rosa, "On the possibility of light string resonances at the LHC and Tevatron from Randall-Sundrum throats", *JHEP* **07** (2009) 77, doi:10.1088/1126-6708/2009/07/077, arXiv:0904.4108.

[13] W. Rarita and J. Schwinger, "On a Theory of Particles with Half-Integral Spin", *Phys. Rev.* **60** (1941) 61, doi:10.1103/PhysRev.60.61.

[14] D. A. Dicus, D. Karabacak, S. Nandi, and S. K. Rai, "Search for spin-3/2 quarks at the Large Hadron Collider", *Phys. Rev. D* **87** (2013) 15023, doi:10.1103/PhysRevD.87.015023.

[15] W. J. Stirling and E. Vryonidou, "Effect of spin-3/2 top quark excitation on $t\bar{t}$ production at the LHC", *JHEP* **01** (2012) 55, doi:10.1007/JHEP01(2012)055, arXiv:1110.1565.

[16] B. Moussallam and V. Soni, "Production of heavy spin-3/2 fermions in colliders", *Phys. Rev. D* **39** (1989) 1883, doi:10.1103/PhysRevD.39.1883.

[17] CMS Collaboration, "Search for pair production of excited top quarks in the lepton + jets final state", *JHEP* **06** (2014) 125, doi:10.1007/JHEP06(2014)125, arXiv:1311.5357.

[18] CMS Collaboration, "The CMS Experiment at the CERN LHC", *JINST* **3** (2008) doi:10.1088/1748-0221/3/08/S08004.

[19] J. Alwall et al., "MadGraph 5: going beyond", *JHEP* **6** (2011) 128, doi:10.1007/JHEP06(2011)128.

[20] NNPDF Collaboration, "Parton distributions for the LHC Run II", *JHEP* **04** (2015) 40, doi:10.1007/JHEP04(2015)040, arXiv:1410.8849.

[21] T. Sjöstrand et al., "An introduction to PYTHIA 8.2", *Comput. Phys. Commun.* **191** (2015) 159, doi:10.1016/j.cpc.2015.01.024.

[22] GEANT4 Collaboration, "Geant4—a simulation toolkit", *Nucl. Instrum. Meth. A* **506** (2003) 250, doi:10.1016/S0168-9002(03)01368-8.

[23] P. Nason, "A New method for combining NLO QCD with shower Monte Carlo algorithms", *JHEP* **11** (2004) 40, doi:10.1088/1126-6708/2004/11/040, arXiv:hep-ph/0409146.

[24] S. Frixione, P. Nason, and C. Oleari, "Matching NLO QCD computations with Parton Shower simulations: the POWHEG method", *JHEP* **11** (2007) 70, doi:10.1088/1126-6708/2007/11/070, arXiv:0709.2092.

[25] S. Alioli, P. Nason, C. Oleari, and E. Re, "A general framework for implementing NLO calculations in shower Monte Carlo programs: the POWHEG BOX", *JHEP* **06** (2010) 43, doi:10.1007/JHEP06(2010)043, arXiv:1002.2581.

[26] J. M. Campbell, R. K. Ellis, P. Nason, and E. Re, "Top-Pair Production and Decay at NLO Matched with Parton Showers", *JHEP* **04** (2015) 114, doi:10.1007/JHEP04(2015)114, arXiv:1412.1828.

[27] H. B. Hartanto, B. Jager, L. Reina, and D. Wackeroth, "Higgs boson production in association with top quarks in the POWHEG BOX", *Phys. Rev. D* **91** (2015) 94003, doi:10.1103/PhysRevD.91.094003, arXiv:1501.04498.

[28] J. Alwall et al., "The automated computation of tree-level and next-to-leading order differential cross sections, and their matching to parton shower simulations", *JHEP* **07** (2014) 79, doi:10.1007/JHEP07(2014)079, arXiv:1405.0301.

[29] R. Frederix and S. Frixione, "Merging meets matching in MC@NLO", *JHEP* **12** (2012) 61, doi:10.1007/JHEP12(2012)061, arXiv:1209.6215.

[30] J. Alwall et al., "Comparative study of various algorithms for the merging of parton showers and matrix elements in hadronic collisions", *Eur. Phys. J. C* **53** (2008) 473, doi:10.1140/epjc/s10052-007-0490-5, arXiv:0706.2569.

[31] CMS Collaboration, "Particle-flow reconstruction and global event description with the CMS detector", (2017). arXiv:1706.04965. Submitted to *JINST.*

[32] M. Cacciari, G. P. Salam, and G. Soyez, "The Anti-k(t) jet clustering algorithm", *JHEP* **04** (2008) 63, doi:10.1088/1126-6708/2008/04/063, arXiv:0802.1189.

[33] CMS Collaboration, "Jet energy scale and resolution in the CMS experiment in pp collisions at 8 TeV", *JINST* **12** (2017) doi:10.1088/1748-0221/12/02/P02014, arXiv:1607.03663.

[34] CMS Collaboration, "Identification of b quark jets at the CMS Experiment in the LHC Run 2", CMS Physics Analysis Summary CMS-PAS-BTV-15-001, 2016.

[35] CMS Collaboration, "Performance of CMS muon reconstruction in pp collision events at $\sqrt{s} = 7$ TeV", *JINST* **7** (2012) 10002, doi:10.1088/1748-0221/7/10/P10002, arXiv:1206.4071.

[36] CMS Collaboration, "Measuring Electron Efficiencies at CMS with Early Data", CMS Physics Analysis Summary CMS-PAS-EGM-07-001, 2008.

[37] Particle Data Group Collaboration, "Review of particle physics", *Chin. Phys. C* **40** (2016) 100001, doi:10.1088/1674-1137/40/10/100001.

[38] K. Cranmer, "Kernel estimation in high-energy physics", *Comput. Phys. Commun.* **136** (2001) 198, doi:10.1016/S0010-4655(00)00243-5.

[39] G. Cowan, K. Cranmer, E. Gross, and O. Vitells, "Asymptotic formulae for likelihood-based tests of new physics", *Eur. Phys. J. C* **71** (2011) 1554, doi:10.1140/epjc/s10052-011-1554-0;10.1140/epjc/s10052-013-2501-z, arXiv:1007.1727.